Supplementary materials for "Self-induced back-action optical pulling force"

Tongtong Zhu[1], Yongyin Cao[1], Lin Wang[1], Zhongquan Nie[2], Tun Cao[3], Fangkui Sun[1], Zehui Jiang[1], Manuel Nieto-Vesperinas[4], Yongmin Liu[5], Cheng-Wei Qiu[6], and Weiqiang Ding[1]

[1] Department of Physics, Harbin Institute of Technology, Harbin 150001, China

[2] Key Lab of Advanced Transducers and Intelligent Control System, Ministry of Education and Shanxi Province, College of Physics and Optoelectronics, Taiyuan University of Technology, Taiyuan 030024, China

[3] Department of Biomedical Engineering, Dalian University of Technology, Dalian 116024, China

[4] Instituto de Ciencia de Materiales de Madrid, Consejo Superior de Investigaciones Científicas, Campus de Cantoblanco, Madrid 28049, Spain

[5] Departments of Mechanical & Industrial Engineering and Electrical & Computer Engineering, Northeastern University, Boston, MA 02115, USA

[6] Department of Electrical and Computer Engineering, National University of Singapore, 4 Engineering Drive 3, Singapore 117583, Singapore

Here, we provide supplementary materials for (1) the contributions of intensity gradient force to the optical pulling in interfacial tractor beam, (2) self-recovering of the SC beam and simultaneous pulling of two objects, and (3) robustness and stability of the pulling force.

1. Intensity gradient force in the interfacial tractor beam (ITB)

In the main text, we concluded that the optical pulling force is quite different from results reported before, because it is mainly determined by an intensity gradient force rather than by a scattering one. In order to illustrate this difference, we use an example the interfacial tractor beam (ITB) as previously reported in (Nat. Photon. 7, 787-790, (2013)). The configuration of the ITB is shown in Fig. S1(a), which is a transparent ellipse floating on the water-air interface. The parameters of the configuration are: $r_x = 2.0\ \mu\text{m}$, $r_y = 0.16\mu\text{m}$, $n_1 = 1.0$, $n_2 = 1.33$, $n_3 = 1.45$, and the incidence angle θ varies within some range.

The total optical force exerted on the object (TM polarization, calculated by a closing surface integration of Maxwell's stress tensor) is shown by the solid blue curve in Fig. S1(b), which is negative within a wide range of angles of incidence. However, the gradient force component $F_{x,\text{grad}}$ is positive (calculated by Eq. (3) in the main text), as shown by the red dashed line. Therefore, the total negative pulling force is not generated by the gradient force. This can be understood by the electric field distribution shown in Fig. S1 (c). For the incidence angle of 12 degrees, (denoted by A and B in Fig. S2(b)), one can find that the object acts like a lens and focuses the incident light gradually inside it, which forms *a positive intensity gradient in +x direction* (i.e. the intensity from *I* to *J increases* gradually). Thus, intensity gradient force component is a pushing one. The differences between the total forces $F_{x,\text{total}}$ and $F_{x,\text{grad.}}$ is due to the scattering force, which is generated by the enhancement of the forward momentum of the photons, scattered from air to water.

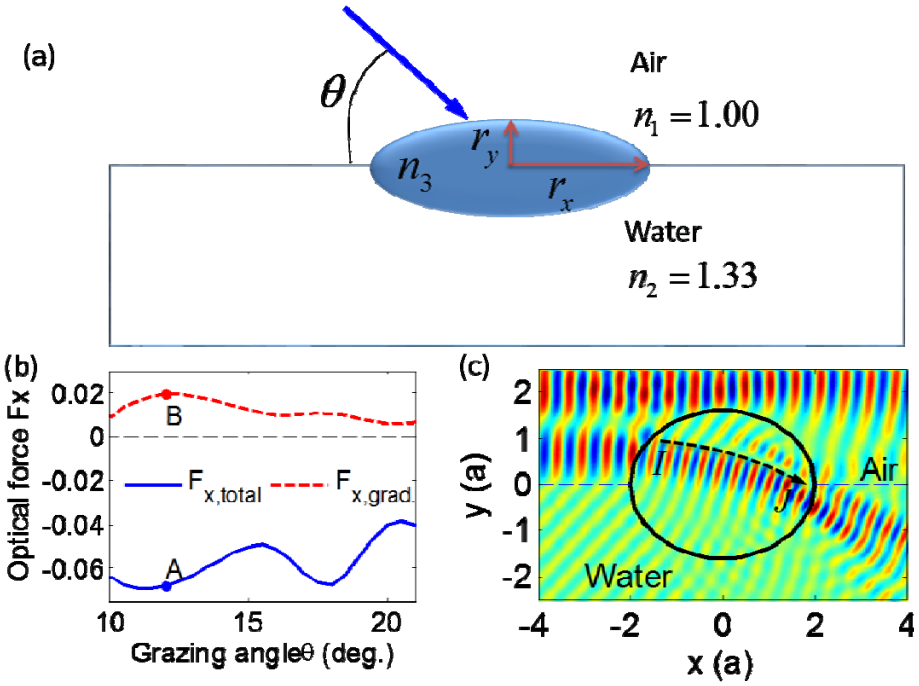

Fig. S1. Intensity gradient force in the interfacial tractor beam configuration. (a) Schematic configuration of the interfacial tractor beam (ITB) reported in (Nat. Photon. 7, 787-790, (2013)). The incident wavelength is $\lambda_0 = 0.532$ μm , and the semi-axes are $r_x = 2.0$ μm and $r_y = 1.6$ um , respectively. (b) Total optical force (blue and solid, and calculated by Eq. (1) in the main text), and gradient force (red and dashed, and calculated by Eq. (3) in the main text) exerted on the object. It is clear that the gradient force is not dominant in the total force. (c) Field distribution of E_z at the case of $\theta = 12^\circ$, which is denoted by the position of A and B in (b).

2. Self-recovering of the SC beam and simultaneous pulling of two objects

The self-recovering property of the SC mode plays an important role in the optical pulling force. Fig. S2 shows the field profiles of the SC modes when the object shifts from $x = 60a$ to $x = 7.5a$ along $-x$ direction. Clearly, one can see that the object (blue ellipses) always locates in the negative intensity gradient region, which generates the continuous optical pulling force. To the right of the object, the SC gradually recovers itself, (with small scattering losses). Initially, the object locates at the position $x = 60a$. When the SC beam is excited, the object will experience a pulling force in -*x* direction, and then it will gradually move towards –*x*. At the same time, the local negative intensity gradient also synchronously shifts with the object, and the force is continuously negative. Since the SC beam can only propagate along the *x* direction, (the scattering into the *y* direction is lost), the SC beam will recover itself, as shown in Fig. S2. The slightly decrease in the amplitude after self-recovering means there's a scattering loss due to the present of the object.

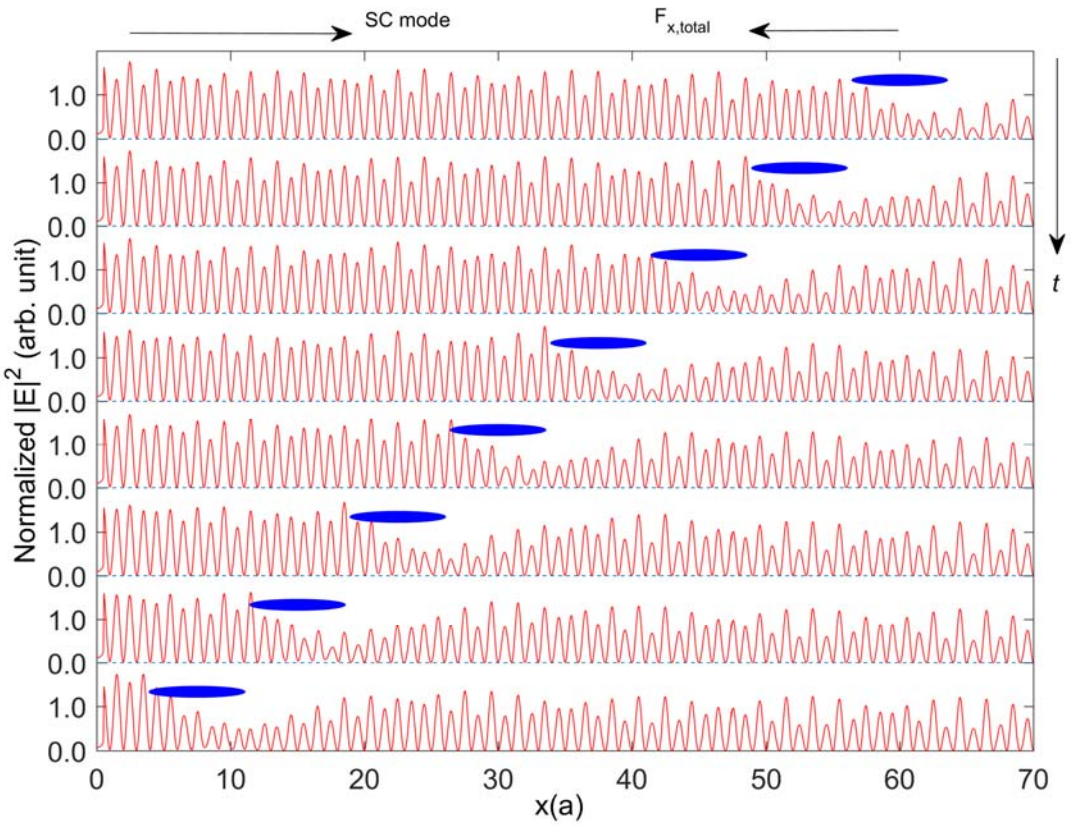

Fig. S2. Self-recovering of the SC mode after being scattered by the object. The initial position of the object is set at $x = 60a$, and then excite the SC mode to illuminate the object, which experiences a negative optical pulling force, moving towards the left. Since the negative intensity gradient force shifts with the object synchronously, the pulling force is continuous and endless. The self-recover of the SC mode can be clearly observed wherever the object is.

In Figure S3, both the objects are identical to the one used in the previous cases. Now, the first object is fixed at $x = 0$ and the second object is shifted d_{12} along the x-axis. Then the total optical forces on both objects are calculated, and the results are shown in Fig. S3a, which shows that the optical forces on both objects are negative. The force on the first object is a negative constant, and this is because it is fixed and does not shift relative to the lattice background. As illustrated in previous section, the SC mode can recover itself when scattered by the first object, thus the second object will experience the recovered SC mode when d_{12} is large enough (larger than $10a$ in current situation). As a result, the force on the second object is also negative and changes periodically with position, just as the case of only one object being pulled. The intensity profiles through both objects are shown in Fig. S3c and S3d, respectively. From these intensity profiles, one can understand the negative forces on both objects. Here, the blue solid curve shows the intensity envelope of the SC mode, and the two arrows, labeled with **F** and **k,** show the direction of the optical force and the mode propagation, respectively.

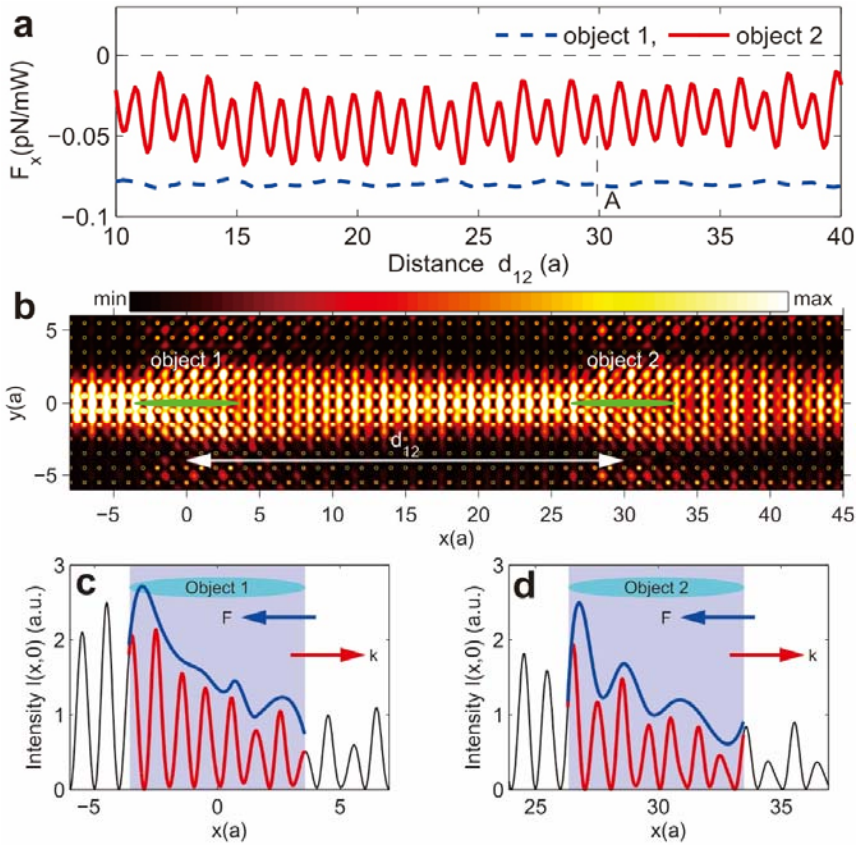

Fig. S3. Simultaneous pulling of two objects. (**a**) Optical forces exerted on the two objects for different center-to-center separation d_{12} between them. Both objects are the same as that used in FIG. 3 (cf. main text). The first object is fixed at x=0, and the second one shifts d_{12} to the right of the first one. The blue curve corresponds to the object 1 and the red curve to the object 2. (**b**) Electric field distribution $|E(x,y)|^2$ with the inter-distance being about 30a (denoted by A in Fig. S5(a)). Both objects experience a negative gradient force, i.e., a pulling force. (**c**) and (**d**) are the electric filed profiles (red curves) around the two objects, superposed to the negative intensity envelope gradient, (blue curves), towards the source.

3. Robustness and stability of the optical pulling force

In the main text, we stated that the pulling force reported here is not difficult to observe in experiment, because it is robust and stable. Here, we provide some results to show these properties, including the insensitivity to the lattice deviation, frequency detune, and lateral stability.

3.1 Robust to geometrical random deviations and frequency detunes

In practice, imperfections of the structure will introduce extra scattering losses and destroy the non-diffracting property of the SC mode. However, we find that the SC mode is very robust, and the self-collimation still exists when random imperfections are introduced in the structure.

In order to illustrate this property, we calculated the SC mode with different kinds of imperfections introduced in the ideal structure. The optimized parameters are $n_a = 3.4$ (refractive index of the

dielectric rods), $n_b = 1.33$ (refractive index of background), $a = 532$ nm (lattice constant), and $r = 53$ nm (radius of the dielectric rods). The operation wavelength (in vacuum) is designed as 1.06 μm.

When we set the incident wavelength being 1.07 μm or 1.05 μm, the non-diffractive property of the mode is still maintained, as shown in Fig. S4(a) and (b), respectively. In Fig. S4(c), we introduce random deviations in the positions of the dielectric rods, i.e., they are positioned at $\left(ia + \delta_x a, ja + \delta_y a\right)$, with $i \in [1,100]$ and $j \in [-10,10]$ being integer numbers, while δ_x and δ_y are normal distributed random numbers with zero expectation value and a standard deviation 0.01, which represents the amplitude of the position random errors. In Fig. S4(d), the radius of the dielectric rods is randomly perturbed as $r = r_0\left(1+\delta_r\right)$. Here $r_0 = 53$ nm is the ideal value of the radius, and δ_r is a normal distribution random number with zero expectation value and standard deviation 0.02. One can find that the SC mode still exists when different random perturbations are introduced. This robustness of the SC mode is very useful in practice.

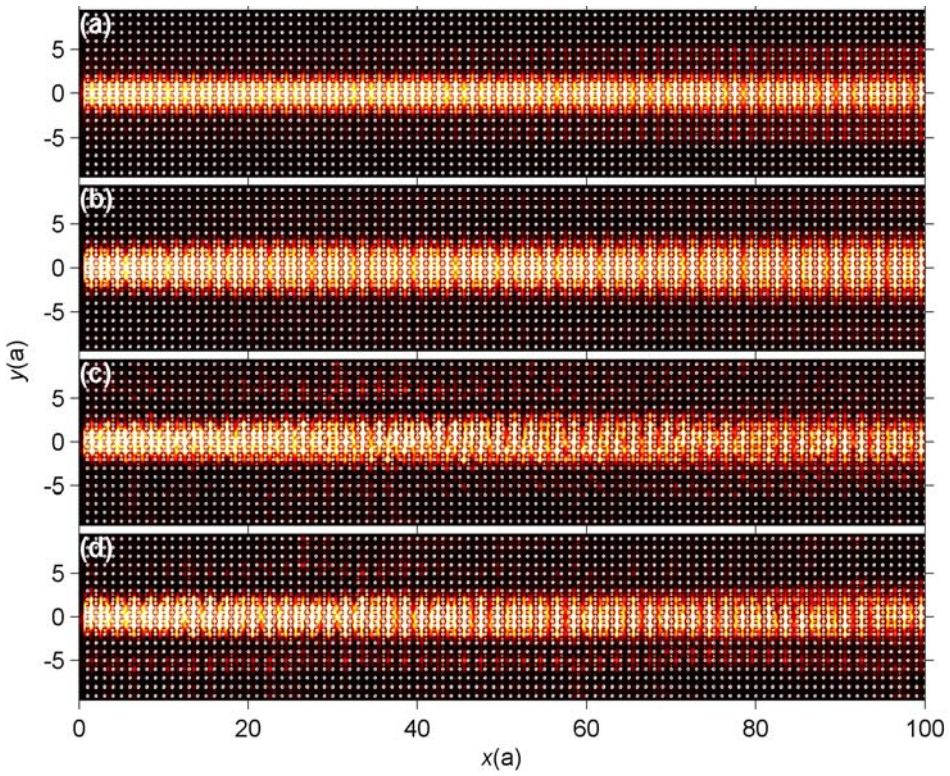

Fig. S4. Robustness of the SC mode to geometrical random deviations and frequency detunes which may be introduced in practice. The SC mode is designed for the wavelength of 1.06 μm, and the parameters are $n_a = 3.4$, $n_b = 1.33$, $a = 532$ nm and $r_0 = 53$ nm. (a) SC mode pattern for a larger wavelength of 1.07 μm. (b) For a smaller wavelength 1.05 μm. (c) Perturbing the positions of the dielectric rods to $(x, y) = \left(ia + \delta_x a, ja + \delta_y a\right)$ with $i \in [1,100]$ and $j \in [-10,10]$ being integers. δ_x and δ_y are normal distributed random numbers with zero expectation and standard deviation 0.01. (d) Perturbing the radius of the dielectric rods to $r_0\left(1+\delta_r\right)$ with $r_0 = 53$ nm. δ_r is a normal distributed with zero expectation and standard deviation 0.02.

3.2. Robustness of F_x to the angle of incidence

According to the analysis in the main text, the self-collimation mode can be excited provided the incident angle θ_{in} is smaller than a critical angle. Fig. S5(a) illustrates that the optical force still remains negative with the same oscillation periodicity, except for a decrease in the force amplitude when the incidence angle increases from 0 to 9 degrees. This feature can be understood from Fig. S5 (b-f), which shows the intensity distribution and profiles for different angles of incidence when the object is centered at $x_{o1} = 1.9a$ (denoted in Fig. S5(a)).

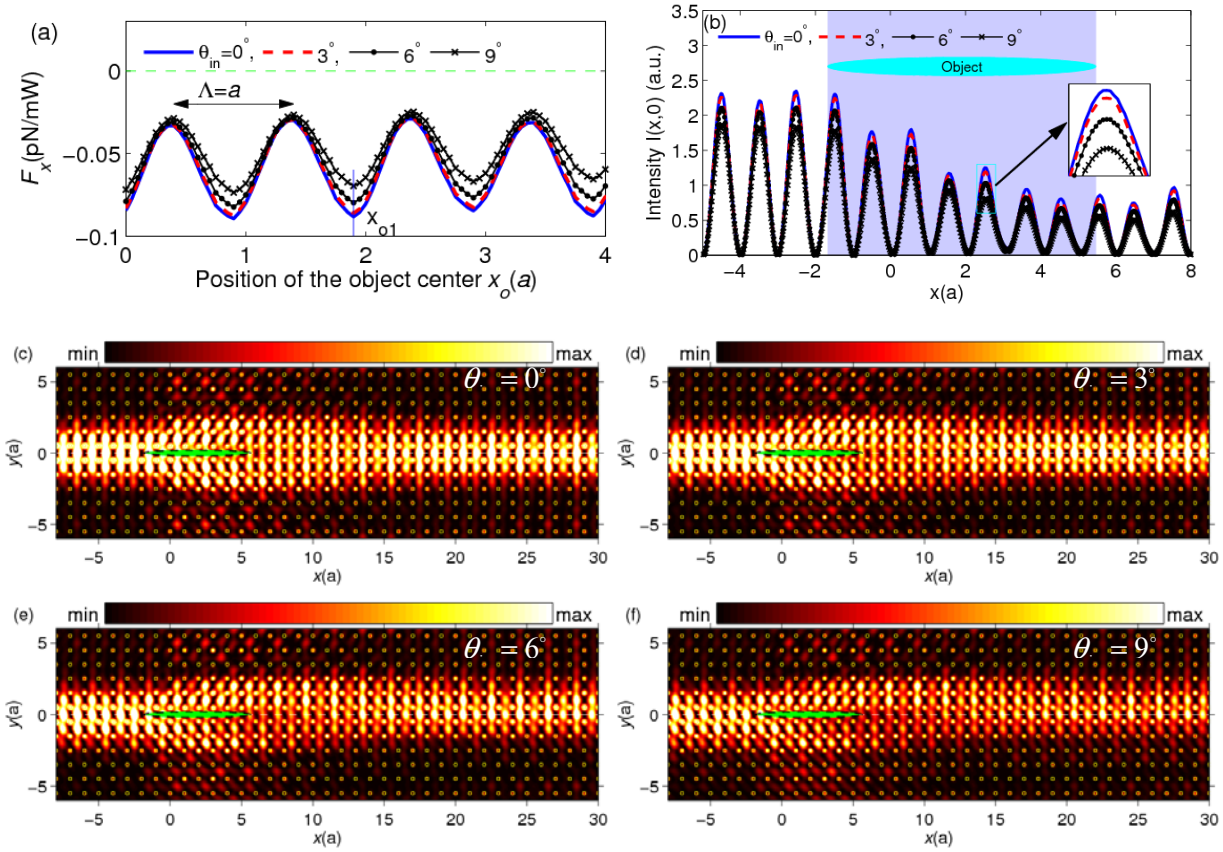

Fig. S5. (a) Optical force for different incidence angles of $\theta_{in} = 0^\circ$ (blue and solid curve), 3° (red and dashed), 6° (solid with dot), and 9° (solid with cross), respectively. All forces have the same oscillation periodicity (equal to the lattice constant), but different maxima and minima. (b) Intensity profiles $I(x,0)$ through the object when it is located at $x_{o1} = 1.9a$ (denoted in (a)) for different incidence angles from 0 through 9 degrees. The intensity envelopes have similar gradient behaviors but different maxima. This agrees well with the tendency of changes of the pulling forces illustrated in (a). (c-f) show the intensity patterns of the angles of incidence from 0° through 9°, respectively.

3.3 Transverse stability of the optical pulling

In the main text, we have comprehensively investigated the continuous and endless optical pulling force in the *x*-direction. On the other hand, the force in the transverse *y*-direction F_y determines the stability of the pulling manipulation. Here, we show that the pulling force is stable when the object is near the SC mode axis of $y=0$, as shown in Fig. S6.

Fig. S6(a) shows transverse shift y_o of the object relative to the SC mode symmetry axis of $y=0$. Fig. S6(b) shows the changes of F_y versus y_o when the object is at $x_{o1}=1.9a$ and $x_{o2}=2.4a$ (x_{o1} and x_{o2} are denoted in FIG. 3(a) of the main text). Clearly, a restoring force F_y in the *y*-direction exists when $y_o \in [-0.1a, 0.1a]$, which can bind the object to the symmetry axis of the SC mode, and avoid the collision of the object with the neighboring PC nanorods. At the same time, within the whole stable region, the pulling force in the *x*-direction F_x only decreases slightly, as shown in Fig. S6(c).

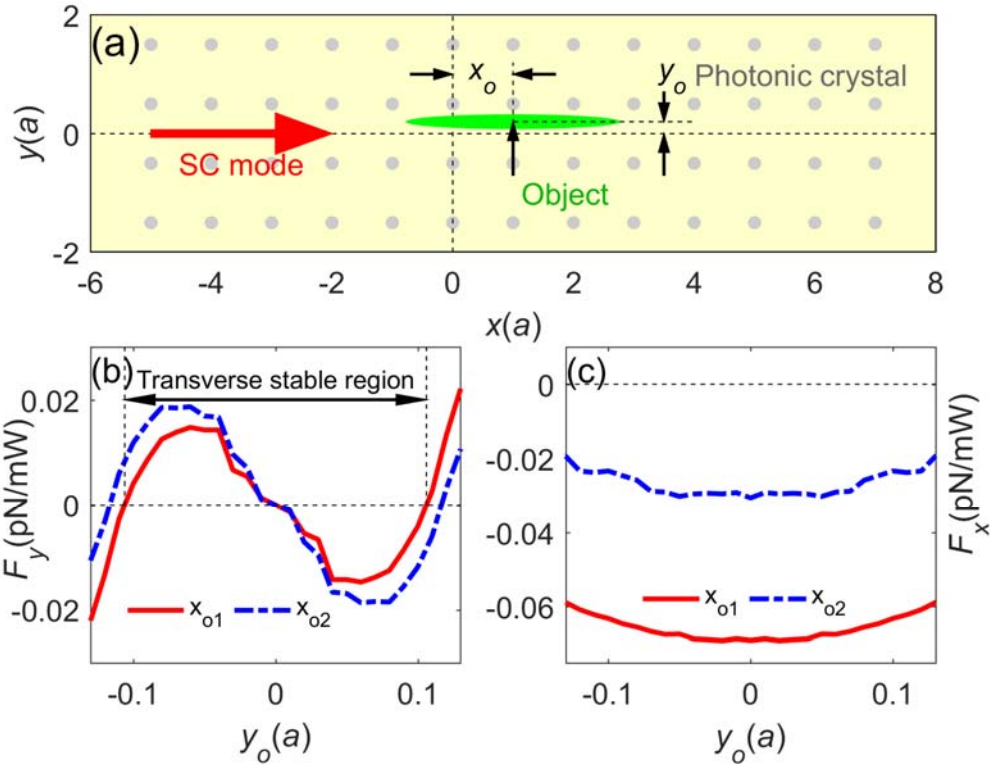

Fig. S6. Transversal stability of the optical pulling manipulation. (a) Schematic of the transverse shift y_o of the object center from the SC mode symmetry axis of $y=0$. The gray dots show the PC lattice background. (b) Transverse force F_y versus y_o when the object is at $x_{o1}=1.9a$ (red and solid curve) and $x_{o2}=2.4a$ (blue and dashed curve) (which are two typical position denoted in FIG. 3 in the main text). The transverse stable region is found to be from $-0.1a$ to $0.1a$. (c) The pulling force F_x versus the transverse shift y_o when the object is at $x_{o1}=1.9a$ (red and solid curve) and $x_{o2}=2.4a$ (blue and dashed curve), respectively.